Accuracy of the Method of Moments for Scattering by a Cylinder

Karl F. Warnick and Weng Cho Chew, *Fellow, IEEE*

***Abstract*—We study the accuracy and convergence of the method of moments for numerical scattering computations for an important benchmark geometry: the infinite circular cylinder. From the spectral decomposition of the electric-field integral equation for this scatterer, we determine the condition number of the moment matrix and the dependence of solution error on the choice of basis functions, discretization density, polarization of the incident field, and the numerical quadrature rule used to evaluate moment-matrix elements. The analysis is carried out for both the TM polarization (weakly singular kernel) and TE polarization (hypersingular kernel). These results provide insights into empirical observations of the convergence behavior of numerical methods in computational electromagnetics.**

***Index Terms*—Boundary integral equations, electromagnetic scattering, error analysis, moment methods, numerical analysis.**

I. Introduction

NUMERICAL methods based on integral equations have enjoyed wide use in computational electromagnetics for many years, and the introduction of techniques for fast evaluation of interactions has greatly extended the range of problems that can be analyzed using integral equation solvers [1]. Despite the increasing importance of these methods, the dependence of solution accuracy on the discretization scheme and the geometry of the scatterer remains poorly understood. In this paper, we study the convergence of the method of moments for a perfectly conducting cylinder.

Asymptotic error and condition number estimates for the boundary-element method applied to the Helmholtz problem have been obtained through the theory of fractional order Sobolev spaces [2]–[7]. These results quantify the dependence of solution convergence rates and operator conditioning on the discretization length, in the limit of infinite refinement. Due to the large electrical sizes of problems of interest in computational electromagnetics, however, asymptotic theories alone are insufficient in validating and improving numerical methods since the dependence of convergence rates on the size and global geometry of the scatterer must be understood as well. *A posteriori* residual-based error bounds have also been developed [8]–[10], and have been applied to adaptive grid algorithms [11]. These bounds require numerical evaluation of Sobolev norms and accurate computation of residuals in order to bound the solution error.

As a consequence of the lack of a satisfactory convergence theory for large scattering problems, numerical methods are validated by checking test cases for which exact or tabulated solutions are available. Although this type of verification can provide reasonable confidence of accuracy over classes of similar scatterer geometries, it yields only a limited understanding of the underlying causes of solution error and condition number growth. Without theoretical insight, numerical observations for test cases can be extrapolated only heuristically to more general problems of practical interest.

In order to illustrate the influences of scatterer size and geometry on the behavior of surface integral-equation methods, and to better understand how benchmark results generalize to more complex problems, we study the accuracy of the method of moments applied to the electric-field integral equation (EFIE) for an infinite circular cylinder from a theoretical point-of-view. For the cylinder, the spectrum of the EFIE is known [12]. We obtain the spectrum of the discretized operator, and thereby determine the condition number of the moment matrix and the solution error in terms of the choice of basis functions, the discretization density, and the numerical quadrature rule used to evaluate moment-matrix elements. Results are given for both the TM polarization (weakly singular kernel) and TE polarization (hypersingular kernel). Spectral analyses of the EFIE have also been given for an infinite strip and cavity [13], [14]. The dependence of the conditioning of the moment matrix on the inner product used to discretize the EFIE has been studied for the cylinder using a similar approach [15].

II. TM Polarization

The EFIE for a TM-polarized time–harmonic electric field $E^i(\mathbf{x})$ incident on a two-dimensional perfectly conducting scatterer is

$$-ik_0\eta \int_S ds'\, g(\mathbf{x},\mathbf{x}')J(\mathbf{x}') = E^i(\mathbf{x}) \tag{1}$$

where S denotes the surface of the scatterer, k_0 is the wavenumber of the incident field, and η is the characteristic impedance of the surrounding medium. The kernel is $g(\mathbf{x},\mathbf{x}') = iH_0^{(1)}(k_0|\mathbf{x}-\mathbf{x}'|)/4$, where $H_0^{(1)}(x)$ is the Hankel function of the first kind. We discretize the EFIE using the moment method by approximating the surface current $J(\mathbf{x})$ as a linear combination of expansion functions $f_n(\mathbf{x})$ and enforcing boundary conditions on the radiated field using the testing functions $t_n(\mathbf{x})$, where the index n ranges from one

Manuscript received May 11, 1999. This work was supported by the Air Force Office of Scientific Research under the Multidisciplinary Research Initiative Grant F49620-96-1-0025.

The authors are with the Center for Computational Electromagnetics, Department of Electrical and Computer Engineering, University of Illinois at Urbana-Champaign, Urbana, IL 61801-2991 USA.

Publisher Item Identifier S 0018-9480(00)08725-1.

to the total number of unknowns N. The continuous integral operator is thereby reduced to the moment matrix

$$Z_{mn} = -ik_0\eta h^{-1} \iint ds\, ds'\, g(\mathbf{x},\mathbf{x}')t_m(\mathbf{x})f_n(\mathbf{x}') \quad (2)$$

where h is the element width or discretization length. The parameter h determines the number of degrees of freedom. In this paper, we employ the dimensionless discretization density or unknowns per wavelength $n_\lambda = \lambda/h$ to characterize the fineness of the mesh.

The results of this paper are based on determining the spectrum of Z_{mn} for the special case of a cylindrical scatterer. The kernel of the EFIE can be expanded in cylindrical modes using

$$H_0^{(1)}(k_0|\mathbf{x}-\mathbf{x}'|) = \sum_{l=-\infty}^{\infty} J_l(k_0a)H_l^{(1)}(k_0a)e^{il(\phi-\phi')} \quad (3)$$

where $\mathbf{x}$ and $\mathbf{x}'$ lie on a circle of radius a and ϕ and ϕ' are the corresponding angles in the cylindrical coordinate system. We assume that the expansion and testing functions are of the form $f_n(\phi) = f(\phi-\phi_n)$ and $t_n(\phi) = t(\phi-\phi_n)$, and that the nodes are evenly spaced so that $\phi_n = (n-1/2)\theta_0$, where $\theta_0 = 2\pi/N$. In terms of cylindrical modes, the moment matrix becomes

$$Z_{mn} = \frac{\eta\pi k_0 a}{2N} \sum_{l=-\infty}^{\infty} J_l(k_0a)H_l^{(1)}(k_0a)T_{-l}F_l e^{il(\phi_m-\phi_n)} \quad (4)$$

where T_l is the Fourier transforms of $t(\phi)$

$$T_l = \frac{1}{\theta_0}\int d\phi\, t(\phi)e^{-il\phi} \quad (5)$$

evaluated at l and normalized by $1/\theta_0$, and F_l is defined similarly.

From (4), the eigenvectors of the moment matrix are of the form $e^{iq\phi_n}$, where q is an integer. The corresponding eigenvalues can be determined from

$$\sum_{n=1}^{N} Z_{mn}e^{iq\phi_n} = \frac{\eta\pi k_0 a}{2N} \sum_{l=-\infty}^{\infty} J_l(k_0a)H_l^{(1)}(k_0a) \times T_{-l}F_l e^{il\phi_m} \sum_{n=1}^{N} e^{i(q-l)\phi_n}. \quad (6)$$

The sum over n can be evaluated using

$$\sum_{n=1}^{N} e^{iq\phi_n} = (-1)^q \frac{\sin(\pi q)}{\sin(\pi q/N)}. \quad (7)$$

The right-hand size of (7) is equal to $(-1)^s N$ if $q = sN$, where s is an integer, and vanishes otherwise. Equation (6) then becomes

$$\sum_{n=1}^{N} Z_{mn}e^{iq\phi_n} = \left[\frac{\eta\pi k_0 a}{2} \sum_{s=-\infty}^{\infty} J_{q+sN}(k_0a)H_{q+sN}^{(1)}(k_0a) \times T_{-q-sN}F_{q+sN}\right] e^{iq\phi_m}. \quad (8)$$

From this expression, we can identify

$$\lambda_q = \frac{\eta\pi k_0 a}{2} \sum_{s=-\infty}^{\infty} J_{q+sN}(k_0a)H_{q+sN}^{(1)}(k_0a) \times T_{-q-sN}F_{q+sN} \quad (9)$$

as the eigenvalue of $e^{iq\phi_n}$. By making use of this result, we will determine the condition number of the moment matrix and the solution error introduced by discretization.

In the limit as $N \to \infty$, the Fourier transforms T_l and F_l become unity, and only the $s = 0$ term of the summation in (9) remains. Thus, the eigenvalues of the moment matrix are of the form

$$\lambda_q = \lambda_q^0 + \Delta_q \quad (10)$$

where $\lambda_q^0 = (\eta\pi k_0 a/2)J_q(k_0a)H_q^{(1)}(k_0a)$ is the corresponding eigenvalue of the continuous integral equation and arises from the $s = 0$ term. The deviation of $T_{-q}F_q$ from unity in the $s = 0$ term of (9), together with the remaining terms of the sum, produce a spectral error term Δ_q due to the discretization of the continuous integral operator. The spectral error will be studied further in Section II-B.

A. Condition Number

The difficulty of solving a linear system with the matrix $\bar{\mathbf{Z}}$ is determined in large part by the condition number of the matrix. The condition number $\kappa(\bar{\mathbf{Z}})$ in the L_2 norm is the ratio of the largest and smallest singular values of the matrix. Since the eigenfunctions of the EFIE for the cylinder are complete, and the operator can be diagonalized by a unitary transformation, it is a normal operator (see [16]). Equation (4) shows that for a regular discretization, the discretized EFIE has a complete system of eigenvectors, and is a normal matrix. The singular values of a normal matrix are equal to the magnitudes of the eigenvalues, thus, we can obtain the condition number from the extremal eigenvalues.

As a function of q, $|J_q(k_0a)H_q^{(1)}(k_0a)|$ is oscillatory and increasing for $|q| < k_0a$, and decays monotonically for $|q| > k_0a$. The maximum value occurs at $|q| \simeq k_0a$. Using expansions of the Bessel and Hankel functions [17, eq. 8.441 #3, eq. 8.443, and eq. 8.454], we arrive at

$$J_\nu(\nu)H_\nu^{(1)}(\nu) \simeq \frac{6^{2/3}(1-i\sqrt{3})}{9\Gamma^2(2/3)}\nu^{-2/3}. \quad (11)$$

From this, the largest eigenvalue of $\bar{\mathbf{Z}}$ is

$$\lambda_{\max} \simeq \frac{\eta 2\pi(1-i\sqrt{3})}{6^{4/3}\Gamma^2(2/3)}(k_0a)^{1/3} \quad (12)$$

where we have neglected the small shift due to discretization error. This eigenvalue corresponds to a surface-wave mode with spatial frequency k_0 on the cylinder. For a large cylinder, this current mode radiates fields that travel in a direction tangential to the surface of the cylinder. The magnitude of the eigenvalue grows with the 1/3 power of the electrical size of the cylinder. By comparison, the eigenvalue of the TM surface-wave mode for an infinite strip grows with the square root of the strip length [13], [14].

The smallest eigenvalue of the moment matrix is more difficult to determine due to the internal resonances associated with closed conducting bodies. It is well known that the EFIE becomes numerically unstable if k_0a is such that the interior boundary value problem with the Dirichlet condition on the surface of the cylinder has a nontrivial solution. In this case, $J_q(k_0a) = 0$ for some integer q. The corresponding eigenvalue of the moment matrix is then determined by the discretization error Δ_q for the resonant mode, and the moment matrix is highly ill conditioned.

If k_0a is such that the condition number of the moment matrix is not dominated by an internal resonance or a near internal resonance, the smallest eigenvalue arises from the highest frequency mode representable in the discrete basis, which corresponds to $|q| = N/2$. Applying the large-order expansion $J_\nu(x)H_\nu^{(1)}(x) \sim -i(\pi|\nu|)^{-1}+O(\nu^{-3}), \nu \to \infty$ [17, eq. 8.452] to $\lambda_{\min} = (\eta\pi k_0a/2)J_{N/2}(k_0a)H_{N/2}^{(1)}(k_0a)$ leads to the result

$$\lambda_{\min} \simeq -\frac{i\eta}{n_\lambda} \tag{13}$$

for the highest order eigenvalue of the moment matrix. As long as n_λ is large enough that this eigenvalue is smaller in magnitude than the lower order eigenvalues, the condition number can be approximated as

$$\kappa(\bar{\mathbf{Z}}) \simeq \frac{\pi 2^{2/3}}{3^{4/3}\Gamma^2(2/3)} n_\lambda (k_0a)^{1/3} \simeq 0.6 n_\lambda (k_0a)^{1/3} \tag{14}$$

by making use of (12) and (13). Since internal resonances cause the magnitude of the smallest eigenvalue of the moment matrix to decrease, this estimate is, in general, a lower bound for the condition number. This condition number estimate is compared to computed values using the singular value decomposition of the moment matrix in Fig. 1.

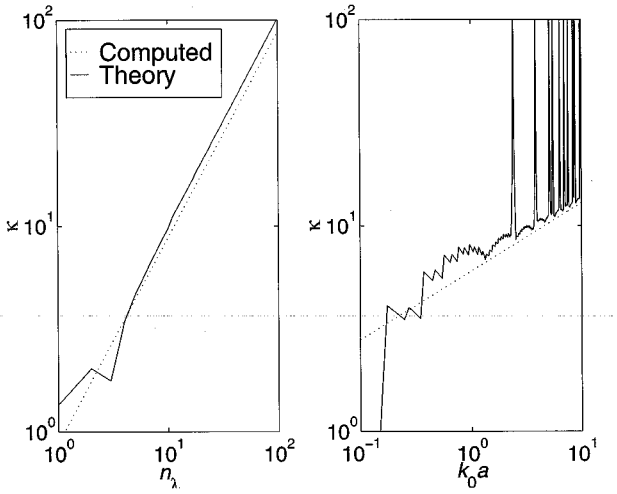

Fig. 1. Condition number of the moment matrix, TM polarization, point testing, and pulse basis function as a function of discretization density n_λ for a cylinder of radius $k_0a = \pi$, and as a function of k_0a for $n_\lambda = 10$.

B. Spectral Error

In this section, we study the spectral error introduced by the discretization of the EFIE, as defined in (10). Using the large-order expansion $J_\nu(x)H_\nu^{(1)}(x) \sim -i(\pi|\nu|)^{-1}$, the spectral error can be approximated by

$$\Delta_q \simeq -\frac{i\eta}{2n_\lambda} \sum_{s\neq 0} \frac{T_{-q-sN}F_{q+sN}}{|s+q/N|} + \lambda_q^0[T_{-q}F_q - 1] \tag{15}$$

where n_λ is the number of unknowns per wavelength. The relative spectral error $E_q = \Delta_q/\lambda_q^0$ is

$$E_q \simeq -\frac{i\eta}{2n_\lambda\lambda_q^0} \sum_{s\neq 0} \frac{T_{-q-sN}F_{q+sN}}{|s+q/N|} + T_{-q}F_q - 1. \tag{16}$$

The first term of this expression is determined by the asymptotic behavior of the spectral representation of the kernel, which is associated with the singularity of the Green's function $g(\mathbf{x}, \mathbf{x}')$ at $\mathbf{x} = \mathbf{x}'$. This contribution to E_q might be called a "sampling error" since it arises from aliasing of high spatial frequency ($|q| > N/2$) components of the kernel. The second term $T_{-q}F_q - 1$ is the approximation error or smoothing error caused by inaccurate representation of low spatial frequency ($|q| \leq N/2$) eigenfunctions of the kernel.

1) Polynomial Bases: We now consider the specialization of (16) to the case of piecewise polynomial expansion and testing functions. The particular basis functions studied here are generated by convolutions of the pulse function, and are splines of the type studied in [15]. As p increases, greater accuracy is obtained by p refinement, for which the basis consists of a set of polynomials complete up to order p, but we do not consider this type of discretization here.

For the piecewise polynomial bases, the product of the Fourier transforms of the testing and expansion functions is $T_{-q}F_q = \mathrm{sinc}^b(q/N)$. The exponent b is equal to $p + p' + 2$, where p and p' are the polynomial orders of the testing and expansion functions. The pulse function (piecewise constant basis) is of order 0, and the triangle function (piecewise linear basis) is order 1. The delta function (point matching) can also be considered in this scheme, and has order -1. In practice, $b \leq 4$ since p refinement is generally employed for polynomial bases beyond first order.

By making use of (16), the spectral error for these types of testing and expansion functions is

$$E_{q,b} \simeq -\frac{i\eta}{2n_\lambda\lambda_q^0} \sum_{s\neq 0} \frac{\mathrm{sgn}(s)\sin^b \pi(s+\beta_q/n_\lambda)}{\pi^b(s+\beta_q/n_\lambda)^{b+1}} + \left[\frac{\sin(\pi\beta_q/n_\lambda)}{\pi\beta_q/n_\lambda}\right]^b - 1 \tag{17}$$

where $\beta_q = q/(k_0a)$ is the normalized spatial frequency of the qth mode. Fig. 2 shows the magnitude of the relative spectral error for a cylinder with a one-wavelength radius and a discretization density of $n_\lambda = 10$. The expression for $E_{q,b}$ is modified slightly for the $b = 0$ case, as described below. For small β_q/n_λ, the spectral error increases with increasing polynomial order of the basis functions. As will be shown in Section II-C, the influence of the spectral error on the current solu-

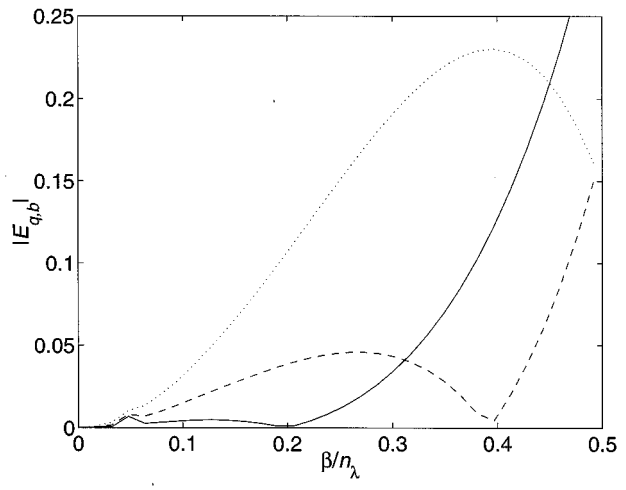

Fig. 2. Relative spectral error $k_0 a = 2\pi$, $n_\lambda = 10$ in terms of $\beta_q/n_\lambda = q/N$, where β_q is the spatial frequency of the qth eigenfunction relative to k_0. Solid line: $b = 0$ (point matching and expansion $\alpha = 1/3$). Dashed line: $b = 1$ (point matching and piecewise constant basis). Dotted line: $b = 2$ (point matching and piecewise linear basis). The spectral error is small for eigenfunctions with low spatial frequency, and is larger near the Nyquist frequency of the mesh ($\beta_q = \pm n_\lambda/2$).

tion error is strongest for $|\beta_q| \leq 1$, which, in Fig. 2, corresponds to $\beta_q/n_\lambda \leq 0.1$.

For the $b = 0$ discretization, the leading order term of the sampling error can be made to vanish by a proper choice of the locations of the delta functions on each element of the discretization. Due to the singularity of the kernel, the testing and expansion points cannot coincide. In order to obtain finite moment-matrix elements, their relative locations must be shifted. We take the testing function to be $\delta(\phi)$ and the expansion function to be $\delta(\phi+\alpha\theta_0/2)/2+\delta(\phi-\alpha\theta_0/2)/2$, where the parameter α specifies the relative shift of the testing and expansion points. In this case, $T_{-q}F_q = \cos(\alpha\pi q/N)$. For small β_q/n_λ, the spectral error evaluates to

$$E_{q,0} \simeq \frac{i\eta \ln[2\sin(\alpha\pi/2)]}{n_\lambda \lambda_q^0} - \frac{i\eta}{4n_\lambda^3\lambda_q^0}\left\{g_3(\alpha) + 2\beta_q^2\left[\frac{\alpha^2\pi^2}{4}g_1(\alpha) + \alpha\pi g_2(\alpha) + g_3(\alpha)\right]\right\} - \frac{\pi^2\alpha^2\beta_q^2}{2n_\lambda^2} \tag{18}$$

where $g_n(x) = i^{n+1}[\mathrm{Li}_n(e^{i\pi x}) - (-1)^n \mathrm{Li}_n(e^{-i\pi x})]$ and $\mathrm{Li}_n(x)$ is the polylogarithm function of order n. In obtaining this result, we have included the third-order term of the expansion $J_\nu(x)H_\nu^{(1)}(x) \sim -i/(\pi|\nu|) - ix^2/(2\pi|\nu|^3)$ in (9). The leading order sampling-error term of (18) vanishes for a shift of $\alpha = 1/3$. In this case, the spectral error becomes

$$E_{q,0} \simeq -\frac{i\eta\left(0.2 + 1.5\beta_q^2\right)}{n_\lambda^3\lambda_q^0} - \frac{\pi^2\beta_q^2}{18n_\lambda^2}. \tag{19}$$

The first term represents sampling error and the second term is the smoothing error.

For pulse expansion functions and point testing ($b = 1$), the spectral error for small β_q/n_λ is

$$E_{q,1} \simeq -\frac{1.8i\eta\beta_q^2}{n_\lambda^3\lambda_q^0} - \frac{\pi^2\beta_q^2}{6n_\lambda^2} \tag{20}$$

where the constant is $3\zeta(3)/2 \simeq 1.8$ and $\zeta(x)$ is the Riemann zeta function. For point testing and triangle expansion functions or pulse testing and expansion functions ($b = 2$), the spectral error is

$$E_{q,2} \simeq -\frac{1.2i\eta\beta_q^2}{n_\lambda^3\lambda_q^0} - \frac{\pi^2\beta_q^2}{3n_\lambda^2} \tag{21}$$

where the constant is $\zeta(3) \simeq 1.2$. For all three discretizations, the sampling error is third order in n_λ^{-1} and the smoothing error is second order. For $b > 2$, the sampling-error term becomes higher order in n_λ^{-1} as b increases. The smoothing error remains second order, but its magnitude grows with b.

2) Quadrature Error: The expressions for the spectral error obtained in the previous section were based on the assumption of exact integration of the moment-matrix elements Z_{mn}. In practice, numerical quadrature rules are employed to evaluate the matrix elements. The effect of approximate integration can be taken into account in (16) by replacing the continuous integral in the Fourier transform of the expansion function $f(\phi)$ with the quadrature rule so that F_q becomes

$$F_{q,M} = \frac{1}{\theta_0}\sum_{n=1}^{M} w_n f(\xi_n) e^{-iq\xi_n} \tag{22}$$

where M is the order of the quadrature rule and w_n are the weights corresponding to the abscissas ξ_n. The Fourier transform T_q of the testing function $t(\phi)$ is modified similarly.

For the M-point first-order Riemann integration rule, the weights are $w_n = \delta = \theta_0/M$ and the abscissas are $\xi_n = (n - 1/2)\delta - \theta_0/2$. In the case of piecewise constant expansion functions ($b = 1$), $F_{q,M}$ becomes the periodic sinc function

$$F_{q,M} = \frac{\sin\dfrac{\pi q}{N}}{M\sin\dfrac{\pi q}{MN}}. \tag{23}$$

The maxima of $F_{q,M}$ lie at $q = MNr$, where $r = 0, \pm 1, \pm 2, \ldots$. Thus, for small q, the terms of the summation over s in (16) for which $s = Mr$ yield the leading contribution to the sampling error. Since $F_{q+sN,M} \simeq (-1)^{r(M+1)}$ for these terms, we find that

$$E_{q,M}^{(1)} \simeq -\frac{i\eta}{2n_\lambda\lambda_q^0}\sum_{r\neq 0}\frac{(-1)^{r(M+1)}}{|Mr|}. \tag{24}$$

If M is even, the sum over r is finite and can be evaluated in closed form, and the sampling error becomes

$$E_{q,M}^{(1)} \simeq \frac{i\eta \ln 2}{Mn_\lambda\lambda_q^0} \tag{25}$$

for small β_q. The quadrature rule also has a small effect on the smoothing error term of the spectral error, but the additional

contribution is of the same order in n_λ as the smoothing error for exact integration.

The quadrature error contribution (25) is first order in n_λ^{-1}, and thus, can dominate the higher order spectral error terms in (16) for small values of M. In order for the quadrature error to be as small as the sampling error in (20) for the $b = 1$ discretization, M must increase as n_λ^2. Commonly, matrix elements near the singularity of the kernel are evaluated using a method such as analytical integration of the singularity of the kernel [18], which reduces the quadrature error significantly. For a single-point integration rule, analytical integration of the diagonal matrix elements reduces the quadrature error roughly by a factor of three for a single-point integration rule [14].

C. Current Error

Once the spectral error due to discretization is known, the surface current solution error can be determined. If the incident field is a plane wave traveling along the x-axis, then the weights J_n, $n = 1, 2, \ldots, N$, of the expansion functions for the approximate current are obtained by solving a linear system with a vector having components

$$E_n^i = \int d\phi\, t_n(\phi) e^{ik_0 a\cos\phi} \tag{26}$$

as the right-hand side. Using the cylindrical mode expansion of a plane wave, E_n^i can be written as

$$E_n^i = \sum_{q=-\infty}^{\infty} i^q J_q(k_0 a) T_{-q} e^{iq\phi_n}. \tag{27}$$

Applying $\bar{\mathbf{Z}}^{-1}$ to this expression gives

$$J_n = \sum_{q=-\infty}^{\infty} \frac{i^q J_q(k_0 a) T_{-q}}{\lambda_q} e^{iq\phi_n} \tag{28}$$

since each term of the sum in (27) is an eigenvector of $\bar{\mathbf{Z}}$. The exact current at the angle ϕ_n on the cylinder is

$$J_n^0 = \sum_{q=-\infty}^{\infty} \frac{i^q J_q(k_0 a)}{\lambda_q^0} e^{iq\phi_n}. \tag{29}$$

The current error $\Delta J_n = J_n^0 - J_n$ is then

$$\Delta J_n = \frac{2}{\eta\pi k_0 a} \sum_{q=-\infty}^{\infty} \frac{i^q(1 + E_q - T_{-q})}{H_q^{(1)}(k_0 a)(1 + E_q)} e^{iq\phi_n}. \tag{30}$$

at the node with angle ϕ_n.

Using this result for the error at each node, the rms current error becomes (31), shown at the bottom of this page.Since the magnitude of $H_\nu^{(1)}(x)$ grows rapidly with $|\nu|$ when $|\nu| > |x|$, the $q \neq 0$ terms of the summation over q in (31) are negligible if $N \gg k_0 a$, which is equivalent to the condition $n_\lambda \gg 1$. We thus arrive at

$$\|\Delta\mathbf{J}\| \simeq \frac{2}{\eta\pi k_0 a} \left[\sum_{q=-\infty}^{\infty} \left| \frac{E_q^{(1)} + T_{-q}(F_q - 1)}{H_q^{(1)}(k_0 a)(1 + E_q)} \right|^2 \right]^{1/2} \tag{32}$$

where $E_q^{(1)}$ is the sampling-error term of (16). This result shows that to leading order, the approximate current solution is not affected by the smoothing error introduced by the testing functions. This occurs because the left- and right-hand sides of the EFIE in (1) are tested using the same set of functions, and the effect of the testing functions cancels for each mode.

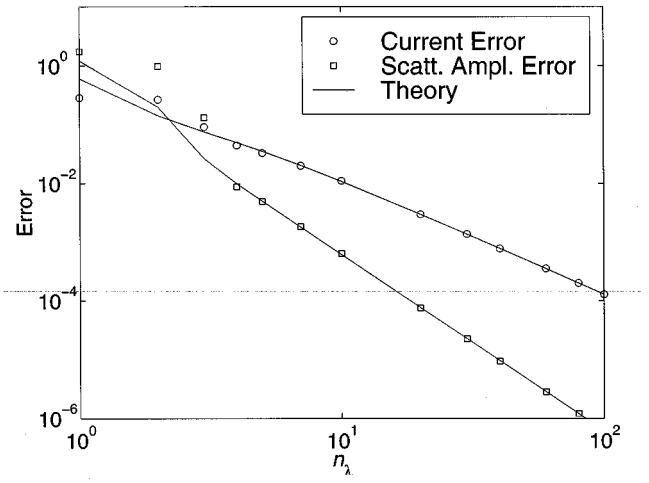

Fig. 3. Relative rms surface current error and backscattering amplitude error for a cylinder, TM polarization, $k_0 a = \pi$, and piecewise constant expansion functions with point testing. The current error is second order, whereas the scattering amplitude error is third order.

A comparison of this result with numerical experiments is shown in Fig. 3. The approximate expression (20) is employed for the sampling error. The number of integration points is sufficiently large that the quadrature error (25) is negligible for this range of n_λ.

Due to the smoothness of the current solution for a smooth incident field, the current error is determined by the spectral error for modes of low spatial frequency, i.e., near k_0 and smaller. This is evident in (32) since the magnitude of the Hankel function grows rapidly with the index when the index is larger than the argument, and terms of the summation in (32) are negligible for $|q| \gg k_0 a$. Modes with higher spatial frequency contribute to the error if the incident field on the surface of the cylinder is less smooth than a plane wave. If the incident field is produced by a line source located at a distance d from the cylinder, for example, then it can be shown that the current error depends on the spectral error E_q for roughly $|q| \leq 2a/d$, for small d,

$$\|\Delta\mathbf{J}\| = \frac{2}{\eta\pi k_0 a} \left[\sum_{q=-\infty}^{\infty} \sum_{s=-\infty}^{\infty} \frac{i^{sN}(1 + E_q - T_{-q})(1 + E_{q+sN}^* - T_{-q-sN}^*)}{H_q^{(1)}(k_0 a) H_{q+sN}^{(1)^*}(k_0 a)(1 + E_q)(1 + E_{q+sN}^*)} \right]^{1/2} \tag{31}$$

which exceeds k_0a when the line source is closer than λ/π to the cylinder.

We consider briefly the behavior of the current error if k_0a is such that the cylinder has an internal resonance or a nontrivial solution to the interior Dirichlet problem. For the continuous EFIE, both the resonant eigenvalue and amplitude of the corresponding mode in the incident field vanish together, as k_0a approaches a resonance, leading to a finite limit for the amplitude of that mode in the exact surface current. For the discretized integral equation, sampling error leads to a nonzero value for the eigenvalue of the resonant mode at the internal resonance. The amplitude of the resonant mode in the discretized incident field (27) is $\tilde{E}_q^i = \sum_{s\neq 0}(-1)^s i^{q+sN} J_{q+sN}(k_0a) T_{-q-sN}$. Since $J_n(x)$ decays exponentially as $|n|$ increases, J_{q+sN} is small for $s \neq 0$, so that $\tilde{E}_q^i$ is negligible in magnitude relative to the sampling error. When the inverse of the moment matrix is applied to $E_{q,n}^i = \tilde{E}_q^i e^{iq\phi_n}$, the resulting approximate current solution is missing the resonant mode. If the discretization error is near the machine precision, then rounding error leads to the corruption of the amplitudes of other modes as well.

Discretization shifts the location of an exact internal resonance of the cylinder as a function of k_0a. At a numerical internal resonance, the moment matrix has an infinite condition number, and direct linear system solution methods can fail due to rounding error. It can also be seen that the numerical internal resonances lie at real values of k_0a, so that discretization does not lead to complex resonances. If χ is a zero of $J_q(x)$, then for k_0a near χ, the eigenvalue of the EFIE of order q can be expanded as

$$\lambda_q^0 \simeq i\frac{\eta\pi\chi}{2} J_q'\chi Y_q(\chi)(k_0a-\chi). \tag{33}$$

From (15), the sampling error Δ_q introduced by discretization is nearly pure imaginary. In order for the eigenvalue $\lambda_q^0+\Delta_q$ of the moment matrix to vanish, (33) shows that $k_0a-\chi$ must be real.

At an exact internal resonance, since the resonant mode is missing from the moment-method solution, the current error is large. Scattering amplitudes and cross sections can still be accurate, however, since an internally resonant mode does not radiate outside the scatterer. At the numerical internal resonance, where the moment matrix is singular, direct solution methods can lead to significant solution error for other modes as well. In this case, the conjugate gradient (CG) iterative solver can be applied to the normal form $\bar{\mathbf{Z}}^\dagger\bar{\mathbf{Z}}\mathbf{J} = \bar{\mathbf{Z}}^\dagger\mathbf{E}$ of the linear system. The amplitude of the resonant mode in the new right-hand side is zero since the corresponding eigenvalue is zero and, thus, the iterative procedure is not significantly affected by the vanishing eigenvalue.

D. Scattering Amplitude Error

For a two-dimensional object, the bistatic scattering amplitude for a plane wave traveling at an angle of ϕ^s due to an incident plane wave is defined by [19]

$$E^s(\rho) \to \sqrt{\frac{-2i}{\pi k_0\rho}} e^{ik_0\rho} S(\phi^i,\phi^s), \qquad \rho\to\infty \tag{34}$$

where E^s is the scattered field, and is related to the scattering width by $\sigma = (4/k_0)|S(\phi^i,\phi^s)|^2$. $S(\phi^i,\phi^s)$ can be obtained from the approximate current J_n on the scatterer using

$$S(\phi^i,\phi^s) = -\frac{\eta\pi k_0a}{2N}\sum_{n=1}^{N} E_n^{s*} J_n \tag{35}$$

where E_n^s is the scattered plane wave, discretized on the surface of the conductor using the expansion functions $f_n(\phi)$.

By making use of (28), the approximate bistatic scattering amplitude for the cylinder becomes

$$S(\phi) = -\sum_{q=-\infty}^{\infty} \frac{J_q(k_0a)F_qT_{-q}}{H_q^{(1)}(k_0a)(1+E_q)} e^{iq\phi} \tag{36}$$

where $\phi = \phi^s - \phi^i$. Subtracting the exact value of the scattering amplitude gives

$$\Delta S(\phi) = -\sum_{q=-\infty}^{\infty} \frac{J_q(k_0a)}{H_q^{(1)}(k_0a)} \frac{E_q^{(1)}}{1+E_q} e^{iq\phi} \tag{37}$$

for the error, where $E_q^{(1)}$ is the sampling-error component of the spectral error E_q. This result shows that to leading order, the smoothing error term $T_{-q}F_q - 1$ of the spectral error E_q does not contribute to the scattering amplitude error. The relative error for the backscattering amplitude $S(0)$ is shown in Fig. 3.

III. TE Polarization

For a TE-polarized incident field, the EFIE becomes

$$-ik_0\eta\hat{\mathbf{t}}\cdot\left[\int_S ds'\, g(\mathbf{x},\mathbf{x}')\mathbf{J}(\mathbf{x}') + \frac{1}{k_0^2}\nabla\int_S ds'\, g(\mathbf{x},\mathbf{x}')\nabla'\cdot\mathbf{J}(\mathbf{x}')\right] = E_t^i(\phi) \tag{38}$$

where $\hat{\mathbf{t}}$ is a unit tangent vector and $\mathbf{J}(\mathbf{x})$ is the surface current vector on the scatterer. The EFIE for the TE polarization differs from the TM EFIE in that the kernel is hypersingular due to the presence of the derivative operators in the second term on the left-hand side of (38).

The TE EFIE can be discretized by employing testing and expansion functions in the same manner as for the TM case. Using the expansion (3), the moment-matrix elements can be expressed as

$$Z_{mn} = \frac{\eta k_0a}{4\theta_0}\iint d\phi\, d\phi'\, t_m(\phi)\sum_l J_l(k_0a)H_l^{(1)}(k_0a) \times\left[\cos(\phi-\phi')f_n(\phi') + \frac{il}{(k_0a)^2}\frac{\partial f_n(\phi')}{\partial\phi'}\right] e^{il(\phi-\phi')} \tag{39}$$

for the circular cylinder. Expanding $\cos(\phi-\phi')$ into exponentials, integrating the second term by parts, and making use of the recursion relations for the derivatives of the Bessel and Hankel functions yields

$$Z_{mn} = \frac{\eta\pi k_0a}{2}\sum_l J_l'(k_0a)H_l^{(1)'}(k_0a)T_{-l}F_l e^{il(\phi_m-\phi_n)}. \tag{40}$$

By proceeding as in the previous section, the eigenvalues of $\bar{\mathbf{Z}}$ are found to be

$$\lambda_q = \frac{\eta\pi k_0 a}{2} \sum_{s=-\infty}^{\infty} J'_{q+sN}(k_0 a) H^{(1)'}_{q+sN}(k_0 a) T_{-q-sN} F_{q+sN} \tag{41}$$

for the TE polarization. This expression is identical to (9), except that the Bessel and Hankel functions are replaced with their first derivatives. The eigenvalues of the continuous EFIE are $\lambda_q^0 = (\eta\pi k_0 a/2) J'_q(k_0 a) H^{(1)'}_q(k_0 a)$.

A. Condition Number

Since $|J'_\nu(x) H^{(1)'}_\nu(x)|$ grows as $|\nu|$ becomes large, in contrast to the TM case, the modes with high spatial frequencies have the largest eigenvalues for the TE polarization. The maximum eigenvalue of $\bar{\mathbf{Z}}$ corresponds to $q = N/2$ and is

$$\lambda_{\max} \simeq \frac{i\eta n_\lambda}{4} \tag{42}$$

where we have made use of $J'_\nu(x) H^{(1)'}_\nu(x) \sim i|\nu|/(\pi x^2), \nu \to \infty$. Near internal resonances lead to small eigenvalues if $k_0 a$ is such that $J'_q(k_0 a)$ is small for some q. These small eigenvalues dominate the condition number for large $k_0 a$. For values of $k_0 a$ such that internal resonances are not dominant, the smallest eigenvalues correspond to the modes with $|q| \simeq k_0 a$, which are the surface-wave modes for the cylinder. In this case, since $J'_\nu \nu H^{(1)'}_\nu(\nu) \simeq 0.2(1 + i\sqrt{3})\nu^{-4/3}$ for large $|\nu|$, the smallest eigenvalue is

$$\lambda_{\min} \simeq 0.3\eta\big(1 + i\sqrt{3}\big)(k_0 a)^{-1/3}. \tag{43}$$

The resulting condition number estimate is

$$\kappa(\bar{\mathbf{Z}}) \simeq 0.4 n_\lambda (k_0 a)^{1/3} \tag{44}$$

which is of the same order as the TM result.

B. Spectral Error

From (41), the relative discretization error is

$$E_q \simeq \frac{i\eta n_\lambda}{2\lambda_q^0} \sum_{s \neq 0} |s + q/N| T_{-q-sN} F_{q+sN} + T_{-q} F_q - 1. \tag{45}$$

The current and scattering amplitude errors have the same forms as (32) and (37) for the TM polarization, but the Bessel and Hankel functions are replaced with their first derivatives. Due to the growth of $H^{(1)'}_\nu(x)$ with ν for $|\nu| > |x|$, the dependence of the error on E_q falls off for $|q| > k_0 a$ for the TE polarization, as occurs for the TM case. Since $H^{(1)'}_\nu(x)$ decreases as $|\nu|$ approaches $|x|$ from below, however, the current error depends more strongly on the spectral error for surface-wave modes with spatial frequencies near k_0 for the TE polarization.

1) Polynomial Bases: If the polynomial basis functions of Section II-B.1 are used to discretize the TE EFIE, the spectral error for the $b = 0$ discretization does not decrease as n_λ becomes large, and the solution does not converge. For the $b = 1$ discretization, the leading order term of the spectral error, as given by (45), vanishes. To obtain the spectral error for small β_q/n_λ, we must employ an additional term of the expansion $J'_\nu(x) H^{(1)'}_\nu(x) \sim i|\nu|/(\pi x^2) - ix^2/(2\pi|\nu|)$ in (41). This leads to

$$E_{q,1} \simeq \frac{0.9 i\eta\beta_q^2}{n_\lambda^3 \lambda_q^0} - \frac{\pi^2 \beta_q^2}{6 n_\lambda^2} \tag{46}$$

where the constant is $3\zeta(3)/4 \simeq 0.9$.

For the $b = 2$ discretization, the diagonal moment-matrix element Z_{nn} diverges if the testing point is located at the apex of the triangle expansion function. The testing functions must be shifted in order for the matrix elements to be finite. Thus, we employ the shifted symmetric testing function $\delta(\phi + \alpha\theta_0/2)/2 + \delta(\phi - \alpha\theta_0/2)/2$. In this case, a factor of $\ln[2\sin(\alpha\pi/2)]$ appears in the leading order term of the sampling error. This term vanishes for a shift of $\alpha = 1/3$, and the total spectral error becomes

$$E_{q,2} \simeq \frac{i\eta\left(-0.2\beta_q^2 + 1.5\beta_q^4\right)}{n_\lambda^3 \lambda_q^0} - \frac{\pi^2 \beta_q^2}{3 n_\lambda^2} \tag{47}$$

for small β_q/n_λ. The constants are $g_4(1/3)/4 \simeq 0.2$ and $\pi g_2(1/3)/6 + g_3(1/3)/2 \simeq 1.5$.

For the $b = 3$ discretization, the spectral error is

$$E_{q,3} \simeq \frac{1.8 i\eta\beta_q^4}{n_\lambda^3 \lambda_q^0} - \frac{\pi^2 \beta_q^2}{2 n_\lambda^2} \tag{48}$$

for small β_q/n_λ. The constant is $3\zeta(3)/2 \simeq 1.8$. In all cases, the sampling error is third order in n_λ^{-1}, and the smoothing error is second order. The sampling errors for the $b = 1$ and $b = 2$ discretizations depend strongly on the location of the testing functions, thus, these discretizations are more sensitive to irregular testing than the $b = 3$ discretization. Fig. 4 gives the spectral error for $1 \leq b \leq 3$. Current error results for the $b = 3$ discretization (pulse testing and triangle expansion functions or point testing with piecewise quadratic expansion functions) are shown in Fig. 5.

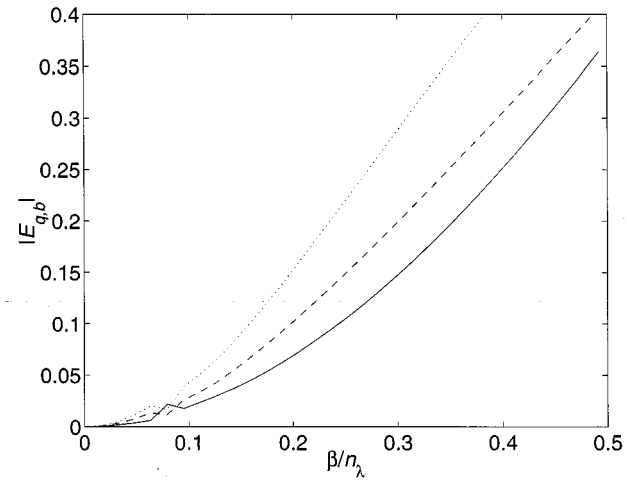

Fig. 4. Relative spectral error TE polarization $k_0 a = 2\pi$, $n_\lambda = 10$ in terms of $\beta_q/n_\lambda = q/N$. Solid line: $b = 1$ (point matching and piecewise constant basis). Dashed line: $b = 2$ (point matching and piecewise linear basis, $\alpha = 1/3$). Dotted line: $b = 3$ (piecewise constant testing functions and piecewise linear basis).

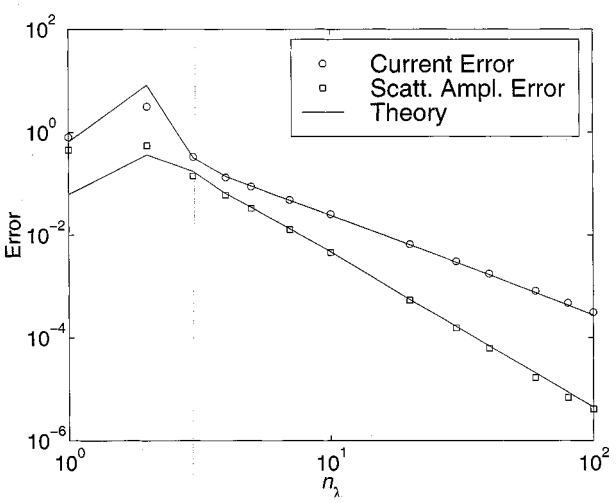

Fig. 5. Relative rms surface current error and backscattering amplitude error for a cylinder, TE polarization, $k_0 a = \pi$, and the $b = 3$ discretization scheme (pulse/triangle or point/quadratic testing and expansion functions).

2) Quadrature Error: Since the kernel of the EFIE for the TE polarization has a stronger singularity than in the TM case, the hypersingular term of (38) is often integrated by parts to reduce the singularity before application of a numerical quadrature rule. We consider here the spectral error introduced by the quadrature rule with and without integration by parts for the case of pulse testing and triangle expansion functions $(b = 3)$ with the M-point integration rule described in Section II-B.2.

If the EFIE is discretized directly as in (38), without integration by parts, the sampling error arising from the hypersingular term is given by

$$E^{(1)}_{q,M} = \frac{i\eta\pi}{2k_0 a\lambda_q^0}\sum_{s\neq 0}(q+sN)J_{q+sN}(k_0 a) \times H_{q+sN}(k_0 a)T_{-q-sN,M}F'_{q+sN,M}. \quad (49)$$

In this expression, $T_{q,M}$ arises from the pulse testing function, and is equal to the periodic sinc function of (23). $F'_{q,M}$ is the Fourier transform of the derivative of the triangle function, sampled using the M-point quadrature rule, which is

$$F'_{q,M} = e^{i\alpha\pi q/N}\frac{2i\sin\dfrac{\pi q}{N}}{\theta_0 \sin\dfrac{\pi q}{MN}} \quad (50)$$

where α specifies the relative shift of the testing and expansion functions. Employing a large-order expansion of $J_\nu(x)H_\nu(x)$ and evaluating the summation over s for small β_q yields

$$E^{(1)}_{q,M} = \frac{\eta\beta_q}{2\lambda_q^0}\tan(\alpha\pi M/2). \quad (51)$$

For $\alpha = 0$, the leading term of the error given by (51) vanishes, and the error becomes higher order in n_λ^{-1}. This result shows that direct integration of the hypersingular term causes sensitivity to irregular testing locations.

With integration by parts, the quadrature error due to the hypersingular term of the EFIE is

$$E^{(1)}_{q,M} = -\frac{\eta\pi}{2k_0 a\lambda_q^0}\sum_{s\neq 0}J_{q+sN}(k_0 a) \times H_{q+sN}(k_0 a)T'_{-q-sN,M}F'_{q+sN,M} \quad (52)$$

where $T'_{q,M}$ is the Fourier transform of the derivative of the pulse function, which is

$$T'_{q,M} = 2i\theta_0^{-1}\sin\frac{\pi q}{N}. \quad (53)$$

Expanding the Bessel and Hankel functions in (52) and evaluating the sum over s leads to

$$E^{(1)}_{q,M} = -\frac{i\eta\beta_q^2}{n_\lambda M\lambda_q^0}\ln\left[2\cos(\alpha\pi M/2)\right] \quad (54)$$

for small β_q, which is of the same order as (25) for the weakly singular kernel. The total sampling error for the TE polarization is given by the sum of (25) and (54). Although the integrand of the hypersingular term has the same spectral content with or without integration by parts, the two formulations differ by a vanishing integral of a total derivative. When a numerical quadrature rule is employed, this integral no longer vanishes, which accounts for the difference between (51) and (54).

IV. Conclusion

From the spectrum of the discretized electric-field integral equation for scattering by a cylinder, we have estimated the condition number of the moment matrix and determined the spectral error introduced by the discretization scheme. For the TM polarization, the largest eigenvalue is determined by the surface-wave mode, and the smallest eigenvalue is produced either by the highest frequency mode representable in the discrete basis or an internally resonant mode. For the TE polarization, the largest eigenvalue is associated with the highest frequency mode, and the smallest eigenvalue is produced by the surface-wave mode or an internal resonance. For both polarizations, neglecting the effect of internal resonances, the condition number grows with the 1/3 power of the electrical size of the cylinder.

The total shift in the spectrum introduced by the discretization of the EFIE divides naturally into two contributions, which we refer to here as sampling and smoothing errors. The first type of error is due to aliasing of high-frequency components of the kernel of the EFIE, and the second arises from inaccurate testing and expansion of low-frequency components of the kernel. We evaluate the spectral error for several types of piecewise polynomial testing and expansion functions and show that, for these discretization schemes, the sampling error is third order, whereas the smoothing error is second order. The use of numerical quadrature to evaluate moment-matrix elements leads to an additional first-order sampling-error contribution. The rms current error on the cylinder at the nodes of the discretization is determined by both the sampling error and the smoothing error due to the expansion functions used to represent the current. The error in scattering amplitudes computed from the current depends on leading order only on the sampling error.

These results on the convergence of the method of moments for the cylinder provide insight into the behavior of numerical methods for more complicated geometries. Since the sampling-error contribution to the spectral shift introduced by discretization is determined locally by the singularity of the kernel, it is relatively independent of the global properties of a scatterer. If the large-scale geometry is such that the spectrum contains small low-order eigenvalues, the relative spectral error becomes large, and moment-method solutions degrade. For the TE polarization, surface —wave modes cause the EFIE to have small eigenvalues, which decrease in magnitude as the size of the scatterer increases. For resonance-regime scatterers, (non-internal) cavity-type resonances are also associated with small eigenvalues of the integral equations of scattering, and large solution errors can occur in this case as well.

REFERENCES

[1] C. C. Lu and W. C. Chew, "A multilevel algorithm for solving a boundary integral equation of scattering," *Microwave Opt. Tech. Lett.*, vol. 7, pp. 466–470, July 1994.

[2] L. Demkowicz, "Asymptotic convergence in finite and boundary element methods: Part 1: Theoretical results," *Comput. Math. Applicat.*, vol. 27, no. 12, pp. 69–84, 1994.

[3] H. Holm and E. P. Stephan, "A boundary element method for electromagnetic transmission problems," *Appl. Anal.*, vol. 56, pp. 213–226, 1995.

[4] H. Holm, M. Maischak, and E. P. Stephan, "The hp-version of the boundary element method for Helmholtz screen problems," *Computing*, vol. 57, pp. 105–134, 1996.

[5] M. Costabel and E. P. Stephan, "A direct boundary integral equation method for transmission problems," *J. Math. Anal. Appl.*, vol. 106, pp. 367–413, 1985.

[6] E. P. Stephan and T. Tran, "Domain decomposition algorithms for indefinite hypersingular integral equations: The h and p versions," *SIAM J. Sci. Comput.*, vol. 19, pp. 1139–1153, July 1998.

[7] E. P. Stephan and W. L. Wendland, "A hypersingular boundary integral method for two-dimensional screen and crack problems," *Arch. Ration. Mech. Anal.*, vol. 112, pp. 363–390, 1990.

[8] E. F. Kuester, "Computable error bounds for variational functionals of solutions of a convolution integral equations of the first kind," *Wave Motion*, vol. 22, pp. 171–185, 1995.

[9] M. Feistauer, G. C. Hsiao, and R. E. Kleinman, "Asymptotic and a posteriori error estimates for boundary element solutions of hypersingular integral equations," *SIAM J. Numer. Anal.*, vol. 33, pp. 666–685, Apr. 1996.

[10] G. C. Hsiao and R. E. Kleinman, "Feasible error estimates in boundary element methods," in *Boundary Element Technology VII*, CA Brebbia and M. S. Ingber, Eds, Southampton: Comput. Mech., 1991, pp. 875–886.

[11] M. Maischak, P. Mund, and E. P. Stephan, "Adaptive multilevel BEM for acoustic scattering," Univ. Hannover, Hannover, Germany, Tech. Rep. IFAM26, Mar. 1997.

[12] S. Amini and N. D. Maines, "Preconditioned Krylov subspace methods for boundary element solution of the Helmholtz equation," *Int. J. Numer. Methods Eng.*, vol. 41, pp. 875–898, 1998.

[13] K. F. Warnick and W. C. Chew, "Accuracy and conditioning of the method of moments for the 2D EFIE," *15th Annu. Rev. Progress Appl. Comput. Electromag.*, pp. 198–204, Mar. 15–20, 1999.

[14] ——, "On the spectrum of the electric field integral equation and the convergence of the moment method," Univ. Illinois at Urbana Campaign, Urbana, IL, Tech. Rep. CCEM-24-99, 1999.

[15] A. G. Dallas, G. C. Hsiao, and R. E. Kleinman, "Observations on the numerical stability of the Galerkin method," *Adv. Comput. Math.*, vol. 9, pp. 37–67, 1998.

[16] A. G. Ramm, "Eigenfunction expansion of a discrete spectrum in diffraction problems," *Radiotekh. Elektron.*, vol. 18, pp. 364–369, 1973.

[17] I. S. Gradshteyn and I. M. Ryzhik, *Table of Integrals, Series, and Products*, 5th ed. New York: Academic, 1994.

[18] S. Wandzura, "Accuracy in computation of matrix elements of singular kernels," in *11th Annu. Rev. Progress Appl. Comput. Electromag.*, vol. II, Monterey, CA, Mar. 20–25, 1995, pp. 1170–1176.

[19] J. J. Bowman, T. B. A. Senior, and P. L. E. Uslenghi, *Electromagnetic and Acoustic Scattering by Simple Shapes*. New York: Hemisphere, 1987.

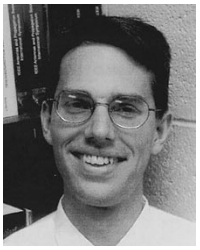

Karl F. Warnick received the B.S. and Ph.D. degrees in electrical engineering from Brigham Young University, Provo, UT, in 1993 and 1997, respectively.

Since 1998, he has been a Research Associate at the Center for Computational Electromagnetics, Department of Electrical and Computer Engineering, University of Illinois at Urbana-Champaign. His research interests include computational electromagnetics, rough surface scattering, and iterative solution methods for large linear systems.

Dr. Warnick was a National Science Foundation Graduate Research Fellow.

Weng Cho Chew (S'79–M'80–SM'86–F'93) received the B.S., the M.S. and Engineer's, and Ph.D. degrees from the Massachusetts Institute of Technology, Cambridge, in 1976, 1978, and 1980, respectively, all in electrical engineering.

He is currently a Professor at the University of Illinois at Urbana-Champaign, and the Director of the Center for Computational Electromagnetics and the Electromagnetics Laboratory. Prior to joining the University of Illinois at Urbana-Champaign, he was a Department Manager and Program Leader at Schlumberger–Doll Research. He is currently a Founder Professor of the College of Engineering at the University of Illinois at Urbana-Champaign. He authored *Waves and Fields in Inhomogeneous Media* (Piscataway, NJ: IEEE Press, 1995), and has co-authored over 200 journal papers, and over 270 conference papers. He is also the originator of several fast algorithms for solving electromagnetics scattering and inverse problems. His research interest is in the area of waves in inhomogeneous media for various sensing applications, integrated circuits, microstrip antenna applications, and fast algorithms for solving wave scattering and radiation problems. He has been active with various journals and societies.

Dr. Chew was a National Science Foundation Presidential Young Investigator and was the recipient of the 2000 IEEE Graduate Teaching Award.